Cover Page

Universiteit Leiden

The handle http://hdl.handle.net/1887/21063 holds various files of this Leiden University dissertation.

Author: Ewing, Mark McConnell
Title: Post-interventional atherosclerotic vascular remodeling : preclinical investigation into immune-modulatory therapies
Issue Date: 2013-05-23

Chapter 11

The lysine acetyltransferase PCAF is a key regulator of arteriogenesis

A.J. Bastiaansen[1,2], M.M. Ewing[1,2,3], H.C. de Boer[2,4], T.C. van der Pouw Kraan[5], M.R. de Vries[1,2], E.A. Peters[1,2], R. Arens[6], S.M. Moore[7], J.E. Faber[7], J.W. Jukema[2,3,8], J.F. Hamming[1], A.Y. Nossent[1,2], P.H. Quax[1,2]

1 Dept. of Surgery, Leiden University Medical Center (LUMC), Leiden, the Netherlands
2 Einthoven Laboratory for Experimental Vascular Medicine, LUMC, Leiden, the Netherlands
3 Dept. of Cardiology, LUMC, Leiden, the Netherlands
4 Dept. of Nephrology, LUMC, Leiden, the Netherlands
5 Dept. of Molecular Cell Biology and Immunology, VU University Medical Center, Amsterdam, the Netherlands
6 Dept. of Immunohematology and Blood Transfusion, LUMC, Leiden, the Netherlands
7 Dept. of Cell and Molecular Physiology, University of North Carolina, Chapel Hill, USA
8 Durrer Institute for Cardiogenetic Research/Interuniversity Cardiology Institute of the Netherlands, the Netherlands.

Submitted for publication

Abstract

Therapeutic arteriogenesis, i.e., expansive remodeling of pre-existing collaterals, using single-action factor therapies has not been as successful as anticipated. Transcriptional co-activator P300/CBP-associated factor (PCAF) has histone acetylating activity and promotes transcription of multiple inflammatory genes. Because arteriogenesis is an inflammation-driven process, we hypothesized that PCAF acts as multifactorial regulator of arteriogenesis.

After induction of hind limb ischemia (HLI), blood flow recovery was impaired in both PCAF$^{-/-}$ mice and healthy wild type (WT) mice treated with the pharmacological PCAF inhibitor Garcinol, demonstrating an important role for PCAF in arteriogenesis. PCAF deficiency reduced the in vitro inflammatory response in leukocytes and vascular cells involved in arteriogenesis. In vivo gene expression profiling revealed that PCAF deficiency results in differential expression of 3505 genes during arteriogenesis and, more specifically, in impaired induction of multiple pro-inflammatory genes. Additionally, recruitment from the bone marrow of inflammatory cells, in particular "pro-inflammatory" Ly6Chi monocytes, was severely impaired in PCAF$^{-/-}$ mice.

These findings indicate that PCAF acts as master switch in the inflammatory processes required for effective arteriogenesis.

Introduction

Peripheral arterial occlusive disease is a leading cause of morbidity and mortality. Blood flow to ischemic tissues in the affected limb can be restored by distinct processes (van Oostrom et al, 2008), namely vasculogenesis, angiogenesis and arteriogenesis, of which arteriogenesis, the remodeling of pre-existing collateral arterioles into larger arteries, has the greatest impact (Heil & Schaper, 2004).
Effective arteriogenesis requires coordination of multiple events. Arteriogenesis is triggered by an increase in fluid shear stress across pre-existing collaterals cross-connecting adjacent arterial trees, which is caused by a pressure gradient created by occlusion or atherosclerotic stenosis of one of the trees. This leads to activation of the endothelial cells and adjacent vascular smooth muscle cells (VSMCs) of the collateral wall. Induction of adhesion molecules, cytokines and chemokines then follows as the first step of an inflammatory cascade essential for arteriogenesis. Recruitment of leukocytes from blood and bone marrow follows, in particular monocytes (Bergmann et al, 2006; Heil et al, 2002; Schaper et al, 1976; Voskuil et al, 2004) but also CD4+, CD8+ and regulatory T cells and natural killer cells (Hellingman et al, 2012; Stabile et al, 2003; Stabile et al, 2006; van Weel et al, 2007; Zouggari et al, 2009). These cells infiltrate into the perivascular space around collaterals and release additional paracrine signaling molecules and growth factors. Subsequent degradation and reorganization of the extracellular matrix by released matrix metalloproteases (MMPs), including MMP2 and MMP9, creates space required for expansive remodeling of the pre-existing collaterals. Proliferation of collateral endothelial cells, VSMCs and fibroblasts is stimulated, resulting in an increased anatomic lumen diameter. All of the steps described above underline the crucial role of inflammation in effective arteriogenesis.
Although stimulation of collateral remodeling is regarded as a promising therapeutic alternative to surgical interventions, clinical trials aimed at modulating individual growth factors or cytokines have thus far not been as successful as anticipated (Schirmer et al, 2009). We now know that the coordinated inflammatory and immune modulatory processes driving collateral growth are multifactorial and too complex to be modulated by therapeutics that target a single gene or pathway. In contrast, modulation of a factor that acts as a master switch for multiple relevant gene programs may be a more effective strategy to augment arteriogenesis.
A recently described protein with such master switch potential is P300/CBP-Associated Factor (PCAF), a transcriptional co-activator with intrinsic histone acetyltransferase activity. PCAF acetylates histones H3 and H4, but there is also increasing evidence that PCAF modulates non-histone proteins (Imhof et al, 1997; Itoh et al, 2000; Liu et al, 1999; Sartorelli et al, 1999), including hypoxia-inducible factor 1α (Hif-1α) (Lim et al, 2010) and Notch (Guarani et al, 2011). Furthermore, the histone acetylating activity of PCAF is essential for NF-κB-mediated gene transcription (Sheppard et al, 1999) and facilitates inflammatory gene regulation (Miao et al, 2004). Since arteriogenesis is an inflammatory-like process, we hypothesized that PCAF acts as master switch that stimulates multiple inflammatory processes important for collateral remodeling.
Recently, it was shown in a large patient population study (>3000 individuals) (Monraats et al, 2005) that a variation in the promoter region of PCAF is associated with

coronary heart disease-related mortality (Pons et al, 2011). In support of this observation, we recently demonstrated a role for PCAF in vascular remodeling in a mouse model for reactive stenosis. However, whether PCAF participates in arteriogenesis has not yet been investigated.
In the present study, we investigated the contribution of PCAF to post-ischemic neovascularization in a hind limb ischemia (HLI) model, using PCAF deficient ($PCAF^{-/-}$) mice. When studying arteriogenesis in a knockout model, it is possible that the gene deletion may affect vascular development in the embryo, including collaterogenesis, thus affecting the number of collaterals available for remodeling after an occlusive event in the adult. To investigate whether observed effects were caused by differences in arteriogenesis, in the native collateral circulation or a combination of both, we examined the pre-existing collateral density as well as the effect of administration of the PCAF inhibitor Garcinol to wild type (WT) mice after induction of HLI. We also studied gene expression and leukocyte recruitment in $PCAF^{-/-}$ and WT mice after induction of HLI to examine potential mechanisms by which PCAF regulates arteriogenesis.

Materials and Methods

Animals

Experiments were approved by the committee on animal welfare of the Leiden University Medical Center (Leiden, The Netherlands). Male C57BL/6 mice were purchased from Charles River (France). The generation of $PCAF^{-/-}$ mice (C57BL/6 background) has previously been described (Duclot et al, 2010; Yamauchi et al, 2000) and the animals were kindly provided by Dr. C. Gongora (Montpellier, France). All animals received regular chow diet and water ad libitum.

Induction of hind limb ischemia

Mice were anesthetized by intraperitoneal (i.p.) injection of midazolam (8 mg/kg, Roche Diagnostics), medetomidine (0.4 mg/kg, Orion) and fentanyl (0.08 mg/kg, Janssen Pharmaceutica). Unilateral HLI was induced by electrocoagulation of the left femoral artery proximal to the superficial epigastric arteries alone, or combined with electrocoagulation of the distal femoral artery proximal to the bifurcation of the popliteal and saphenous artery (Hellingman et al, 2010). After surgery, anesthesia was antagonized with flumazenil (0.7 mg/kg, Fresenius Kabi), atipamezole (3.3 mg/kg, Orion) and buprenorphine (0.2 mg/kg, MSD Animal Health). For pharmacological PCAF inhibition in WT mice, 20 µl 40% pluronic gel (Sigma-Aldrich) with or without 25 mg/ml Garcinol (Santa Cruz Biotechnology) was applied topically to the adductor muscle before skin closure.

Laser Doppler perfusion imaging

Hind limb perfusion was measured with laser Doppler perfusion imaging (LDPI) (Moor Instruments) after intraperitoneal injection of midazolam (8 mg/kg) and medetomidine (0.4 mg/kg). The regions of interest analyzed consisted of the foot distal to the base of the first digit. Perfusion was expressed as the ratio of ligated to non-ligated foot. After measurement, anesthesia was antagonized with flumazenil (0.7 mg/kg) and atipamezole (3.3 mg/kg).

Pre-existing collateral density

Pre-existing collateral density in the pial circulation of the dorsal cerebral cortex predicts collateral density in skeletal muscle and other vascular beds (Chalothorn et al, 2010; Wang et al, 2010; Zhang et al, 2010). However, unlike in other tissues where arterial trees are arranged three-dimensionally and difficult to image with fidelity, all cerebral collaterals are contained within the pia and can thus be directly identified and counted. Methods for measurement of collateral density between the anterior cerebral artery (ACA), middle cerebral artery (MCA), and posterior cerebral artery (PCA) were described elsewhere (Chalothorn et al, 2010; Wang et al, 2010; Zhang et al, 2010). Briefly, animals were heparinized systemically and anesthetized with ketamine (100 mg/kg) and xylazine (10 mg/kg) prior to vascular casting. Maximal dilation was accomplished by cannulation of the thoracic aorta and infusion of sodium-nitroprusside (30 µg/ml) and papaverine (40 µg/ml) in PBS at 100 mmHg for 3 minutes. Yellow Microfil™ (Flow Tech Inc.) with viscosity adjusted to prevent capillary and venous filling was infused under a stereomicroscope after craniotomy. The dorsal cerebral circulation was fixed with topical application of 4% paraformaldehyde to prevent any reduction in vessel dimensions after Microfil injection. Brains were incubated in Evans Blue (2 µg/ml) for several days to improve contrast for visualization of the vasculature. Digital images were obtained at 13X (Leica) of the dorsal brain surface and processed with ImageJ software (NIH). Collateral density was calculated by determining the total number of pial collaterals between the ACA-MCA, ACA-PCA and MCA-PCA and dividing by the dorsal surface area of the cerebral hemispheres. Areas that sustained damage, were incompletely filled, or were otherwise uncountable were excluded from analysis.

Immunostaining and analysis

Mice were sacrificed and the adductor muscle group medial to the femur was excised en bloc. Tissues were snap frozen in liquid nitrogen or fixed in 3.7% formaldehyde. Serial 5-µm-thick paraffin-embedded sections were used for histological analysis of collateral artery number and size. Vessels at the midpoint of the adductor muscle group, stained using anti-smooth muscle α-actin (αSMA) (DAKO), are likely composed of collaterals but may also include arterioles of the opposing tree. Randomly photographed images through the central part of the adductor muscle group were used to quantify the number and lumen diameter of αSMA+ vessels using ImageJ software (total of 9 images of 3 sections per mouse). To correct for non-perpendicularly cut sections, the circular lumen area of αSMA+ vessels was calculated from the lumen diameter measured at the narrowest point.

Frozen 5-µm-thick sections were fixed in ice-cold acetone and stained with anti-PCAF (Abcam) and Cy3 conjugated anti-αSMA (Sigma-Aldrich). PCAF was visualized using Alexa 488 conjugated secondary antibody (Invitrogen). Nuclei were stained using Vectashield with DAPI (Vector Laboratories). Fluorescent images were taken on a LSM700 microscope (Carl Zeiss) and contrast-stretched using Zen 2009 software (Carl Zeiss). Collaterals were detected with Cy3 conjugated anti-αSMA, and perivascular monocytes with anti-MOMA-2 (Millipore), visualized using Alexa 488 conjugated secondary antibody (Invitrogen). Monocytes were quantified from at least six consecutive sections per mouse and expressed as the number of MOMA-2

positive cells in the perivascular space of αSMA+ vessels.

In vitro immune response

Whole blood

Blood was collected from the tail vein of PCAF$^{-/-}$ and WT mice and diluted 1:25 with RPMI 1640 (Invitrogen) supplemented with non-essential amino acids (PAA Laboratories) and glutamax (Invitrogen). Blood was incubated overnight at 37ºC, 5% CO_2, in the presence of lipopolysaccharide (LPS) (0-500 ng/ml) from Escherichia coli K-235 (Sigma-Aldrich). Cell-free supernatant was collected and TNFα level was measured by ELISA (BD Biosciences).

Splenocytes

Spleens were isolated from PCAF-/- and WT mice, minced through a 40µm-cell strainer (Biosciences) and, after erythrolysis with ammonium chloride solution, single cell suspensions were resuspended in DMEM (PAA Laboratories) supplemented with 10% heat-inactivated FCS (Lonza). Splenocytes ($1x10^6$) from PCAF$^{-/-}$ and WT mice were plated and incubated for 24 hours with LPS (300 ng/ml) or control. Splenocytes of WT mice were also incubated with Garcinol (20 µM) in combination with LPS (300 ng/ml) or control. MCP-1 level in the cell-free supernatant was measured by ELISA (BD Biosciences).

Vascular smooth muscle cells

VSMCs were isolated from abdominal aortas from PCAF$^{-/-}$ and WT mice. For stimulation assays, cells (passage 2-4) were plated ($5x10^3$) and incubated for 24 hours with LPS (0.1 and 1 ng/ml) or control. VSMCs of WT mice were also incubated with Garcinol (15 µM) in combination with LPS (0.1 and 1 ng/ml) or control. MCP-1 level in the cell-free supernatant was measured by ELISA (BD Biosciences). RNA was isolated from LPS stimulated (1 ng/ml) WT and PCAF$^{-/-}$ VSMCs ($1x10^5$) using RNeasy minikits (Qiagen).

Whole-genome expression

The adductor muscle group of PCAF$^{-/-}$ and WT mice was harvested before (t0) and 1 day after (t1) induction of HLI, and total RNA was extracted using RNeasy fibrous tissue minikit (Qiagen). RNA integrity was checked by NanoDrop 1000 Spectrophotometer (NanoDrop Technologies) and 2100 Bioanalyzer (Agilent Technologies). For whole-genome expression profiling, amplified biotinylated RNA was generated using the Illumina TotalPrep RNA Amplification Kit. For array analysis, MouseWG-6 v2.0 Expression Beadchips (Illumina), which contain more than 45,200 transcripts, were used. Expression levels were Log_2-transformed and after quantile normalization, transcripts showing background intensity, both at baseline and after induction of HLI, were removed from the analysis. Gene expression levels at t1 were expressed relative to average baseline levels generating t1/t0avg ratios for all 15,555 regulated genes, and compared between both mouse strains. To define the effect of PCAF on inflammatory gene transcription, gene descriptions, as provided by Illumina, containing any of these criteria (interleukin, chemokine, interferon, TGF, TNF, NF-κB) were selected and ratios were tested for significance.

Real-time quantitative PCR

RNA was reverse transcribed using High Capacity RNA-to-cDNA kit (Applied Bio-

systems). Quantitative PCR was performed on the ABI 7500 Fast system, using commercially available TaqMan gene expression assays for HPRT1, MCP-1, MMP9, TNFα, CCL9, CXCL12 and IRF7 (Applied Biosystems).

Flow cytometry

Blood, spleen, bone marrow and non-draining lymph nodes were harvested before (t0) and 1 day after (t1) induction of HLI. Draining lymph nodes were dissected from the inguinal region. Total circulating leukocytes were measured using the KX-21N Hematology Analyzer (Sysmex). Tissues were minced through a 40µm-cell strainer (BD Biosciences) to obtain single cell suspensions which were resuspended in IMDM (Lonza) with 2% FCS. For dendritic cell-specific cell surface staining, the spleen and lymph nodes were first perfused with collagenase (1mg/ml) and DNase (0.02mg/ml) for 10 minutes and minced. Erythrocytes were lysed and samples for intracellular staining were permeabilized. Fluorochrome-conjugated monoclonal antibodies specific for CD3, CD4, CD8, CD11c, CD11b, CD19, CD25, CD86, CD115, FoxP3, Ly6C, Ly6G, B220, DX5 were used. Cells were measured on a LSRII flow cytometer (BD Biosciences) and data was analyzed using FlowJo software (Tree Star, Inc.).

Statistical analysis

All results are presented as mean ± standard error of the mean (SEM) or as scatter plot. Comparisons between groups were performed using Student's T-test. All statistical analyses were performed using SPSS 17.0 software. P-values < 0.05 were considered statistically significant and are indicated with *; p-values < 0.01 and < 0.001 are indicated by ** and ***, respectively. Statistical Analysis of Microarray data (SAM) (Tusher et al, 2001) was used for the analysis on t1/t0avg ratios in the whole-genome expression array. A false discovery rate (expressed as q-values) of less than 5% was considered significant.

Results

PCAF contributes to collateral remodeling

PCAF$^{-/-}$ mice showed impaired blood flow recovery after HLI (Fig 1A-B). Postoperative blood flow was decreased to approximately 6% of blood flow in the contralateral limb in both groups, with a trend towards reduced blood flow in PCAF$^{-/-}$ mice compared to WT mice (Fig 1C, p=0.07). Thereafter, blood flow recovery in PCAF$^{-/-}$ mice was reduced and did not recover completely before termination at 28 days. Moreover, PCAF$^{-/-}$ mice showed significantly more necrotic toe nails than WT mice (PCAF$^{-/-}$ 2.9 ±0.6 vs WT 0.45±0.2, p<0.001) (Fig 1D). No auto-amputation of hind limb digits was observed in either group. The reduced blood flow recovery in PCAF$^{-/-}$ mice was confirmed by quantification of αSMA+ vessels in the adductor muscle group, 28 days after HLI (Fig 1E). Although the number of αSMA+ vessels was nearly similar (Fig 1F), the size of αSMA+ vessels in PCAF$^{-/-}$ mice was significantly reduced, resulting in a reduced blood flow. The mean lumen area per αSMA+ vessel (PCAF$^{-/-}$ 139±15µm^2 vs WT 297±26µm^2, p<0.001) and total lumen area per section (PCAF$^{-/-}$ 447±46µm^2 vs WT 1253±117µm^2, p<0.001) were severely reduced in PCAF$^{-/-}$ mice (Fig 1G-H). Thus, PCAF deficiency leads to reduced arteriogenesis after induction of HLI.

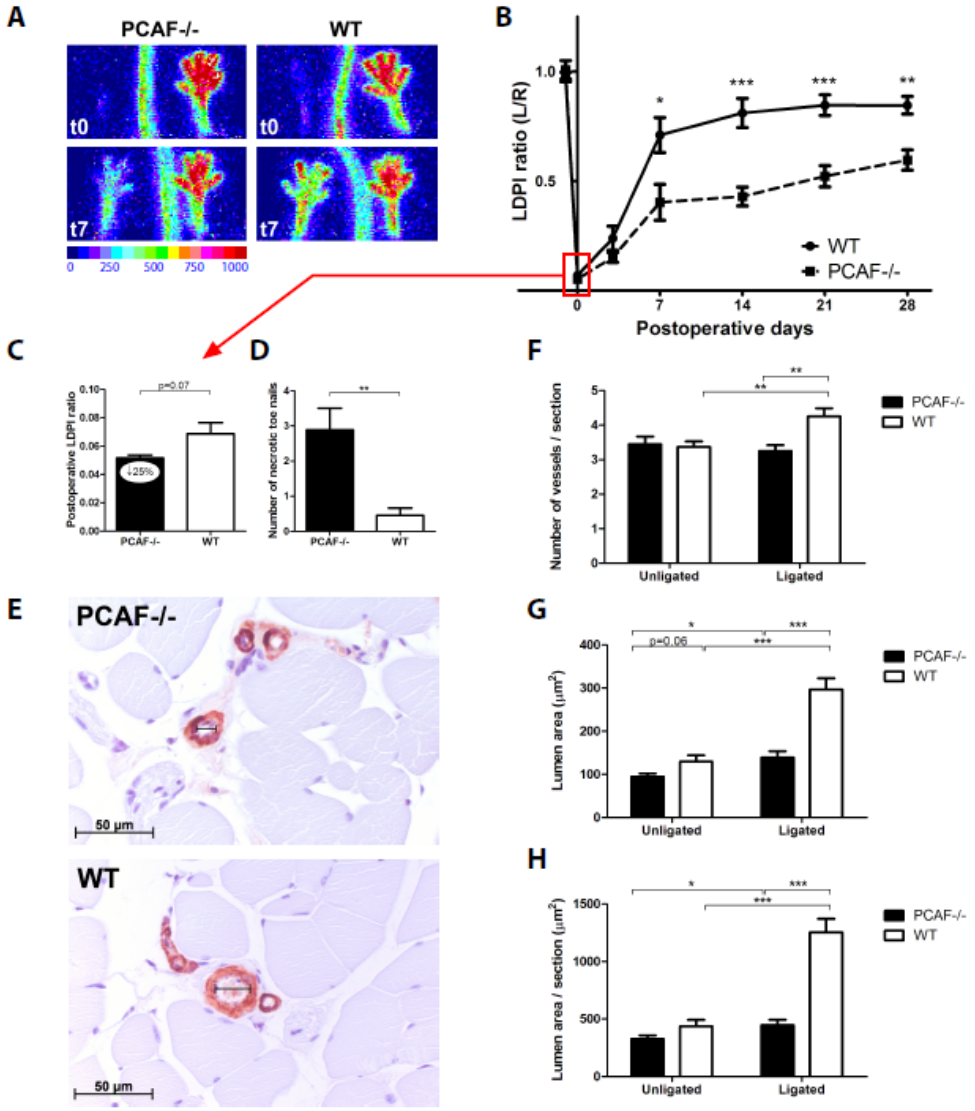

Figure 1. Arteriogenesis in PCAF$^{-/-}$ mice. A. Representative LDPI images of paws from PCAF$^{-/-}$ and WT mice directly and 7 days after induction of HLI in the left limb. High blood flow is displayed in red. B. Quantification of LDPI measurements of PCAF$^{-/-}$ and WT mice over time. Data are calculated as the ratio of ligated over non-ligated paw. C. Quantification of LDPI measurements of PCAF$^{-/-}$ and WT mice directly after induction of HLI. Data are calculated as the ratio of ligated over non-ligated paw. D. Quantification of necrotic toe nails of the ligated limb in PCAF$^{-/-}$ and WT mice counted 28 days after HLI. E. Immunohistochemical staining of paraffin-embedded adductor muscle group of PCAF$^{-/-}$ and WT mice 28 days after HLI using anti-αSMA (red) antibodies. Lumen diameter of αSMA+ vessels is indicated by black bars. Scale bars = 50 µm. F-H. Number, mean lumen area (µm^2) and total lumen area per section (µm^2 / section) of αSMA+ vessels, measured at the center of the adductor muscle group in ligated and non-ligated limbs of PCAF$^{-/-}$ and WT mice. All values are presented as the mean ± SEM. *P < 0.05, **P < 0.01, ***P < 0.001.

To assess whether the reduction in blood flow recovery in PCAF$^{-/-}$ mice was caused by reduced collateral remodeling or by fewer pre-existing collaterals, we performed

two additional experiments. First, we inhibited PCAF by pharmacological intervention with Garcinol to rule out any effects on number of pre-existing collaterals in the PCAF$^{-/-}$ mice. In WT mice, local PCAF inhibition by Garcinol resulted in reduced blood flow restoration compared to the empty pluronic gel control group (Fig 2A-B).

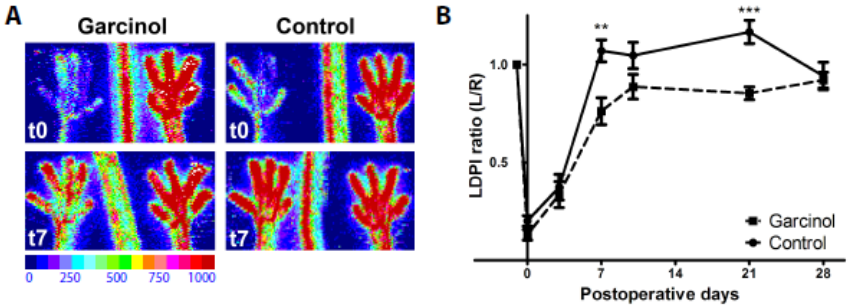

Figure 2. Arteriogenesis after pharmacological inhibition of PCAF. A. Representative LDPI images of paws directly and 7 days after induction of HLI in the left limb. In WT mice, pluronic gel with or without 25 mg/ml Garcinol was applied topically to the adductor muscle before skin closure. High blood flow is displayed in red. B. Quantification of LDPI measurements of WT mice treated with Garcinol or control over time. Data are calculated as the ratio of ligated over non-ligated paw. All values are presented as the mean ± SEM. **P < 0.01, ***P < 0.001, Garcinol versus control.

Secondly, the pre-existing vascular bed of PCAF$^{-/-}$ and WT mice was assessed in the pial circulation using an arterial vascular casting (Fig 3A). Pial collateral density in PCAF$^{-/-}$ mice was reduced by 11% compared to WT mice, reflecting a moderate but significant contribution of PCAF in determining the abundance of the native collateral circulation (Fig 3B-C, p=0.02). This was in agreement with the trend towards decreased blood flow perfusion in PCAF$^{-/-}$ mice directly after HLI.

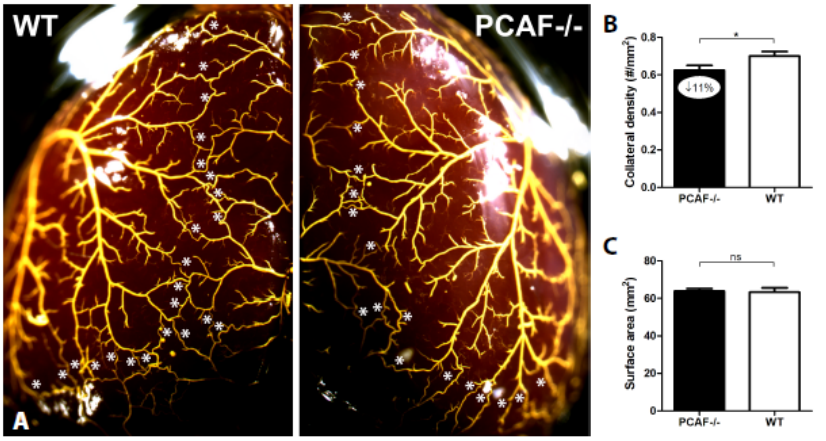

Figure 3. Pre-existing collateral bed in PCAF$^{-/-}$ mice. A. Representative images of the pial circulation in PCAF$^{-/-}$ and WT mice. White asterisks indicate collateral arteries between anterior, middle and posterior cerebral arteries (ACA, MCA and PCA, respectively). Following exsanguination and maximal dilation of the dorsal cerebral circulation, Microfil™ was used as a casting agent, after which the whole brain was fixated in 4% PFA. B. Pial collateral density was calculated in PCAF$^{-/-}$ and WT mice by dividing the sum of ACA to MCA, ACA to PCA and MCA to PCA by the surface area of the cerebral hemispheres. C. Region of the brain utilized for calculation of pial density. Areas were excluded when they were damaged, had poor filling with Microfil™, or were otherwise uncountable. NS = non-significant. All values are presented as the mean ± SEM. *P < 0.05, PCAF-/- versus WT.

PCAF is required for in vitro inflammatory response

We investigated the role of PCAF in the inflammatory response of multiple cell types, given the above evidence for decreased collateral remodeling and the known involvement of these cells in arteriogenesis. Analysis of circulating cells in a whole blood LPS stimulation assay showed dose-dependent increase of TNFα in blood from WT mice, which was significantly reduced in blood from PCAF$^{-/-}$ mice (Fig 4A). Next, the splenic cell reservoir was subjected to LPS stimulation and pharmacological PCAF inhibition with Garcinol. LPS (300 ng/ml)-stimulated MCP-1 levels of splenocytes from both PCAF$^{-/-}$ mice (63±32pg/ml) and WT splenocytes treated with 20 μM Garcinol (195±35 pg/ml) were both significantly reduced in comparison to WT splenocytes (372±13 pg/ml, p=0.005 and p=0.04 respectively) (Fig 4B). Also the inflammatory phenotype of PCAF$^{-/-}$ VSMCs was assessed. Similar to the splenocyte stimulation, MCP-1 levels were markedly reduced after LPS (0.1 ng/ml) stimulation of PCAF$^{-/-}$ VSMCs (689±49 pg/ml) and WT VSMCs when exposed to 15μM Garcinol (3087±284 pg/ml) compared with untreated WT VSMCs (4175±264 pg/ml, p<0.001 and p=0.049 respectively) (Fig 4C). In addition, upregulation of MCP-1 mRNA was significantly reduced by 53% in PCAF$^{-/-}$ VSMCs (Fig 4D, p=0.01). To exclude non-specific effects of Garcinol, these experiments were repeated in WT VSMCs treated with siRNAs against PCAF mRNA instead of Garcinol. Transfection with siRNAs targeting PCAF mRNA efficiently decreased PCAF mRNA expression by 61% and, like Garcinol, inhibited MCP-1 production (Supporting Information Fig 1A-C).

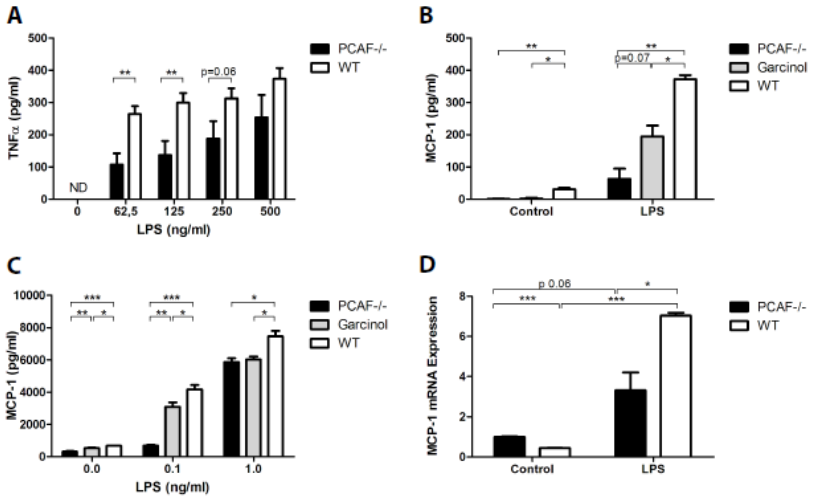

Figure 4. The role of PCAF in in vitro inflammatory response. A. Inflammatory response of whole blood from PCAF$^{-/-}$ and WT mice was evaluated. Blood from tail vein was collected, diluted (1:25) and incubated 24 h with LPS (0-500 ng/ml). TNFα (pg/ml) level in cell-free supernatant was measured by ELISA. ND = non-detectable. B. Splenocytes of PCAF$^{-/-}$ and WT mice were cultured and incubated for 24 h with LPS (300 ng/ml) or control. Splenocytes of WT mice were also incubated with Garcinol (20 μM) in combination with LPS (300 ng/ml) or control. Cell-free supernatant MCP-1 (pg/ml) level was measured by ELISA. C. VSMCs of PCAF$^{-/-}$ and WT mice were cultured and incubated for 24 h with LPS (0.1 and 1 ng/ml) or control. VSMCs of WT mice were also incubated with Garcinol (15 μM) in combination with LPS (0.1 and 1 ng/ml) or control. Cell-free supernatant MCP-1 (pg/ml) level was measured by ELISA. D Vascular smooth muscle cells (VSMCs) of PCAF$^{-/-}$ and WT mice were cultured and incubated for 24 h with LPS (1 ng/ml) or control. MCP-1 mRNA expression was measured by real-time quantitative PCR. Cts were normalized against Cts of HPRT1. All values are presented as the mean ± SEM of triplicates. *P < 0.05, **P < 0.01, ***P < 0.001.

PCAF modulates post-ischemic gene regulation

PCAF staining showed enhanced expression in cells of large developing collaterals in the adductor muscle group compared to surrounding skeletal muscle (Fig 5A). To study differential gene expression after HLI between PCAF$^{-/-}$ and WT mice, total RNA isolated from the adductor muscle group was used in a whole-genome expression analysis using Illumina Beadchips. Statistical analysis by SAM on t1/t0avg ratios identified 1963 genes with a significant lower ratio and 1542 genes with a higher ratio in PCAF$^{-/-}$ relative to WT mice (q<5%), indicating that PCAF exhibits a large effect on gene transcription after HLI (Fig 5B).

Supporting Information Table 1 shows the top 50 genes with impaired upregulation in PCAF$^{-/-}$ mice compared to WT mice, including MMP9, critical in matrix degradation required for collateral artery expansion. Since PCAF has been shown to regulate inflammatory gene transcription, we selected inflammatory genes that were significantly regulated (Supporting Information Table 2 and Supporting Information Fig 2). Among the inflammatory genes showing a more pronounced induction in WT mice compared to PCAF$^{-/-}$ mice were genes encoding cytokines CXCL12, CCL9 and TNFα, chemokine receptor CXCR1, transcription factor IRF7, TNF receptor associated factors TRAF2 and TRAF3, TNF receptor associated protein TRAP1 and members of the TNF receptor superfamily TNFRSF19 and TNFRSF11a (also known as RANK). The total of inflammatory genes with greater induction in PCAF$^{-/-}$ mice was much smaller than the number of genes more strongly induced in WT, and included inhibitors of the NF-κB pathway like NFKBIA and NKIRAS1. Aberrant regulation of several relevant regulated factors (MMP9, TNFα, CCL9, CXCL12, IRF7) were confirmed using real-time quantitative PCR (Fig 5C-G).

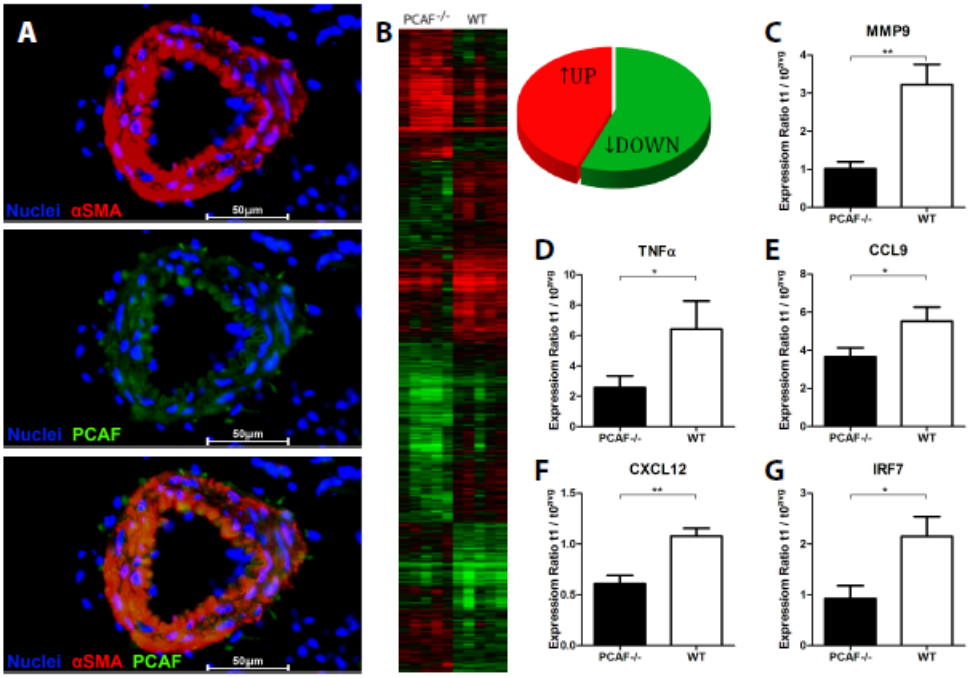

Figure 5. Gene regulation in PCAF$^{-/-}$ mice after HLI. A. Immunohistochemical staining on fresh frozen sections of WT adductor muscle 1 day after HLI, using anti-αSMA (red) and anti-PCAF (green) antibodies. Cell nuclei were stained with DAPI (blue). Scale bars = 50 μm. B. Heatmap of differentially regulated genes in whole-genome expression analysis, comparing PCAF$^{-/-}$ and WT mice. Included are genes that were significantly different between PCAF$^{-/-}$ and WT mice (q-value < 5). Data are presented as the fold change in expression between day 1 (t1) and average preoperative baseline levels (t0), generating t1/t0avg ratios. Red indicates increased and green indicates reduced expression relative to average baseline levels. The pie graph illustrates a significant decrease of 1963 genes (green) and increase of 1542 (red) genes in PCAF$^{-/-}$ relative to WT mice. C-G. Microarray validation by real-time quantitative PCR of a selection of relevant regulated inflammatory factors MMP9, TNFα, CCL9, CXCL12 and IRF7. Cts were normalized against Cts of HPRT1. All values are presented as the mean ± SEM. *P < 0.05, **P < 0.01, PCAF$^{-/-}$ versus WT.

PCAF deficiency alters leukocyte recruitment

We quantified leukocyte subtypes that are involved in arteriogenesis, including T cells (helper CD4+, cytotoxic CD8+ and regulatory T cells) and natural killer cells, and subtypes which have not been previously implicated in arteriogenesis, including B cells and dendritic cells. Blood samples from before (t0) and 1 day after (t1) HLI, were analyzed by FACS. PCAF deficiency had effects on most of the leukocyte subtypes examined. Following HLI, circulatory T cells were significantly decreased in PCAF$^{-/-}$ mice compared to WT mice. This difference was caused mainly by a reduction in CD4+ T cells, especially by the fraction of activated CD4+ T cells, defined by the loss of CD62L (L-selectin), and regulatory T cells (CD4+CD25+FoxP3+ T cells). The number of circulatory CD8+ T cells did not differ between WT and PCAF$^{-/-}$ mice. Also counts of other leukocyte subtypes, including B cells and natural killer cells were decreased by PCAF deficiency.

To investigate the migratory behavior of the leukocyte subtypes, the spleen, bone marrow and lymph nodes were harvested from both mouse strains before (t0) and 1 day after (t1) HLI. Compared to WT mice, we observed reduced numbers of dendritic cells in the draining inguinal lymph nodes of PCAF$^{-/-}$ mice after HLI. Accordingly, the fraction of dendritic cells expressing the co-stimulatory molecule CD86+ was smaller in the draining lymph nodes of PCAF$^{-/-}$ mice. Furthermore, nearly all tested leukocytes subtypes were increased in the bone marrow of PCAF$^{-/-}$ mice compared to WT mice, including CD4+ and CD8+ T cells, natural killer cells and dendritic cells, suggesting that these subpopulations are retained in the bone marrow of PCAF$^{-/-}$ mice during recovery after HLI (Supporting Information Fig 3A-I).

Because monocytes play a key role in arteriogenesis and are among the first leukocytes recruited to remodeling collaterals, we evaluated different monocyte populations in blood, spleen and bone marrow. After HLI, the absolute number of circulating monocytes in WT mice was equal to baseline numbers, but monocytes in PCAF$^{-/-}$ mice significantly decreased compared to baseline (PCAF$^{-/-}$ 0.13±0.05x10^6/mL vs WT 0.37±0.02x10^6/mL, p=0.002) (Fig 6A). In WT mice, the monocyte population increased in the spleen and decreased in the bone marrow after HLI. In contrast, bone marrow monocytes in PCAF$^{-/-}$ mice increased compared to baseline and were significantly higher after HLI compared to WT mice (Fig 6B-C). The differences in monocyte numbers were caused mainly by the specific subtype of “pro-inflammatory” Ly6Chi monocytes (Fig 6D-F). The activation state of total and Ly6Chi monocytes did not differ between the two strains, measured by mean fluorescent intensity of the adhesion molecule CD11b (Fig 6G-H).

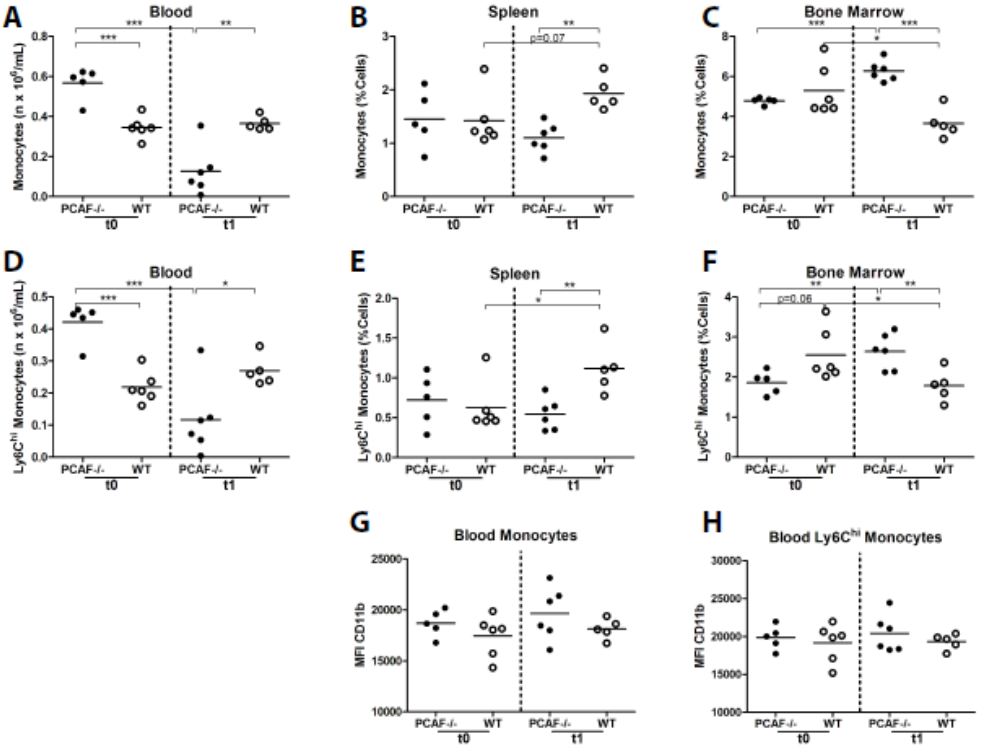

Figure 6. Monocyte recruitment in PCAF$^{-/-}$ mice after HLI. A-C. Flow cytometry analysis of monocytes before (t0) and 1 day after (t1) HLI in PCAF$^{-/-}$ and WT mice. Values are presented as total monocyte counts in blood (nx10^6/mL), spleen (% of total cells) and bone marrow (% of total cells). D-F. Flow cytometry analysis of "pro-inflammatory" Ly6Chi monocytes after HLI in PCAF$^{-/-}$ and WT mice. Values are presented as total Ly6Chi monocyte counts in blood (nx10^6/mL), spleen (% of total cells) and bone marrow (% of total cells). G-H. Activation state of monocytes and Ly6Chi monocytes measured by mean fluorescence intensity (MFI) of CD11b. *P < 0.05, **P < 0.01, ***P < 0.001.

Finally, we assessed the number of monocytes/macrophages in the adductor muscle group by fluorescent staining with antibodies against MOMA-2 and smooth muscle α-actin (Fig 7A). Although PCAF$^{-/-}$ mice showed a significant increase in MOMA-2-positive cells 24 hours after HLI, the increase in WT mice was significantly higher (PCAF$^{-/-}$ 3.2±0.35/section vs WT 6.0±0.43/section, p=0.001) (Fig 7B). Differences were most evident in the perivascular space of remodeling collaterals (PCAF$^{-/-}$ 1.4±0.16/section vs WT 3.5±0.76/section, p=0.01) (Fig 7C).

Discussion

We demonstrate that blood flow recovery after induction of HLI is strongly impaired in PCAF$^{-/-}$ mice, in association with reduced expansive remodeling of collaterals. Furthermore, local PCAF inhibition by Garcinol in WT mice also reduces recovery, indicating that PCAF is directly required for normal arteriogenesis. PCAF gene deficiency results in a repressed in vitro inflammatory response in many cell types known to be involved in arteriogenesis. One day after induction of HLI, 3505 genes are differentially regulated in the adductor muscle group of PCAF$^{-/-}$ mice compared to

WT mice. Additionally, recruitment of different pro-arteriogenic leukocyte subtypes in PCAF$^{-/-}$ mice, in particular “inflammatory” monocytes, is significantly impaired at this time. Our data therefore demonstrate that PCAF plays a key role in post-ischemic arteriogenesis.

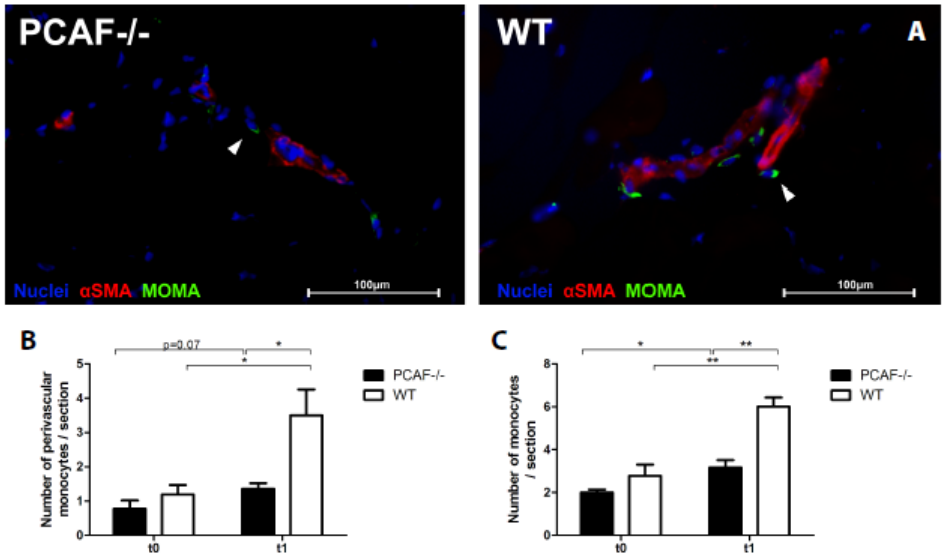

Figure 7. Monocyte recruitment to collateral arteries in PCAF$^{-/-}$ mice after HLI. A. Immunohistochemical staining on fresh frozen sections of the adductor muscle group from PCAF$^{-/-}$ and WT mice 1 day after HLI, using anti-αSMA (red) and anti-MOMA-2 (green) antibodies. Cell nuclei were labeled with DAPI (blue). Scale bars = 100 µm. B-C. Quantification of MOMA-2 positive cells in the adductor muscle group of PCAF$^{-/-}$ and WT before (t0) and 1 day after (t1) HLI. Monocytes were quantified from at least six consecutive sections per mouse and expressed as the number of MOMA-2 positive cells per section and as the number of MOMA-2 positive cells in the perivascular space of αSMA+ vessels per section. *P < 0.05, **P < 0.01.

Compared to WT mice, PCAF$^{-/-}$ mice showed an impaired blood flow recovery after HLI. Our findings suggest that two deficiencies caused by a lack of PCAF are involved. First, the expansive remodeling of αSMA+ arterioles at the center of the adductor muscle group, of which most are collaterals, was reduced by 53% in PCAF$^{-/-}$ mice compared to WT mice. Correspondingly, local application of PCAF inhibitor Garcinol in healthy WT mice also resulted in impaired blood flow recovery compared to control animals. Hence, PCAF has a major impact on arteriogenesis. Secondly, we observed that the density of native pre-existing collaterals in the pial circulation of PCAF$^{-/-}$ mice was reduced by 11%. Even changes of this magnitude have significant effects on collateral-dependent perfusion of tissue downstream from an arterial obstruction (Chalothorn & Faber, 2010; Wang et al, 2010; Zhang et al, 2010). Previous studies have shown that genetic-dependent variation in collateral number in the cerebral pial circulation is shared, at least qualitatively, by similar differences in collateral density in other tissues (Chalothorn et al, 2010; Wang et al, 2010; Zhang et al, 2010). Accordingly, we also observed a trend towards a decrease in blood flow directly after induction of HLI in PCAF$^{-/-}$ mice. In mice, the density of the native collaterals in tissues varies widely among strains from differences in genetic background (Chalothorn et al, 2010; Wang et al, 2010; Zhang et al, 2010). Hence, besides collateral remodeling, genetic PCAF deficiency also contributes to reduced formation of

the collateral circulation which occurs during embryonic development.
In a clinical setting, the outcome after an ischemic event varies among individuals, and differences in abundance of the native collateral circulation have also been reported in patients (Meier et al, 2007; Menon et al, 2012). Moreover, a previous study found that the -2481G allele in the promoter region of the PCAF gene associates with an increased risk of mortality in patients with coronary heart disease (Pons et al, 2011), which further supports our findings that PCAF deficiency impairs collateral function.
In order for PCAF to serve as a master switch in collateral remodeling, it needs to impact multiple critical phases in the process, namely activation of the endothelium and vessel wall, leukocyte recruitment, matrix degradation and arteriolar expansion. We examined gene expression in the adductor muscle group containing remodeling collaterals in the initial phase after HLI. Over 3500 genes were differentially regulated between PCAF$^{-/-}$ and WT mice. This suggests that PCAF impacts expression of a large number of genes activated in this setting. More specifically, PCAF$^{-/-}$ mice showed impaired induction of multiple pro-arteriogenic and pro-inflammatory genes, including matrix metalloproteinase (MMP) 9 and chemokines CXCL12 (SDF1) and CCL9.
MMP9 is critical in degradation and remodeling of the extracellular matrix allowing cell migration and outward expansion of the collaterals and thus effective arteriogenesis (Huang et al, 2009). CXCL12 is elevated in ischemic skeletal muscle of patients with critical limb ischemia (Ho et al, 2010) and acts as chemoattractant for CXCR4+ cells, including leukocytes and progenitor cells. CXCL12-mediated recruitment of bone marrow-derived cells to ischemic tissues results in enhanced neovascularization (Hiasa et al, 2004; Shao et al, 2008). Also CCL9, which is a strong chemoattractant for bone marrow derived cells (Yang & Odgren, 2005), is upregulated after muscle injury (Shireman, 2007).
In addition, PCAF$^{-/-}$ mice showed impaired induction of multiple factors related to the pro-inflammatory TNFα pathway (Silke & Brink, 2010). TNFα$^{-/-}$ mice have reduced collateral artery perfusion (Hoefer et al, 2002) and anti-TNFα therapy attenuates arteriogenesis (Grundmann et al, 2005). Thus, reduced TNFα expression in PCAF$^{-/-}$ mice likely contributes to the impaired arteriogenesis in these mice. Our data suggest that PCAF regulates many factors that have previously been described to play an important role in both inflammation and arteriogenesis (Lee et al, 2004).
It should be noted that RNA was isolated from the adductor muscle group as a whole (Lee et al, 2004) and not from the embedded collateral arteries alone, as was described previously (Dai & Faber, 2010). In that report, a whole-genome microarray analysis was performed on collaterals microdissected from the gracilis muscle 24 hours after HLI. Here we found exceedingly more differentially expressed genes, then the 404 genes that were found upregulated in gracilis collaterals of WT mice (Dai et al, 2010). Using the entire adductor muscle group for microarray analysis, not only the collaterals but also infiltrating leukocytes and surrounding non-vascular tissues were included in these analyses.
As discussed in the introduction, an inflammatory-like process plays a role in all stages of arteriogenesis. To investigate the impact of PCAF on the inflammatory response of the different cell types involved in arteriogenesis, we studied circulating cells in whole blood, splenic leukocytes and VSMCs in vitro. PCAF is critical for

the regulation of transcription factor NF-κB, that consists of a p65 and p50 subunit bound to inhibitory proteins in the cytoplasm. Upon stimulation NF-κB is translocated to the nucleus and regulates the expression of multiple genes, including TNFα and MCP-1 (Lenardo & Baltimore, 1989; Miao et al, 2004). PCAF binds to the NF-κB p65 subunit and activates NF-κB-related inflammatory gene expression (Miao et al, 2004; Sheppard et al, 1999). We clearly demonstrate that PCAF deficiency results in decreased production of pro-inflammatory cytokines by multiple cell types after stimulation with LPS. LPS stimulated whole blood from PCAF$^{-/-}$ mice produced less TNFα than blood from WT mice, indicating a reduced inflammatory phenotype of circulating cells. Also PCAF$^{-/-}$ cells isolated from the spleen, one of the major leukocyte reservoirs, showed a reduced inflammatory response compared to splenocytes from WT mice. PCAF$^{-/-}$ VSMCs produced less MCP-1 than WT VSMCs in response to LPS, which would favor reduced monocyte recruitment and therefore reduced VSMC proliferation, which is essential for collateral remodeling. We obtained similar results using either Garcinol or PCAF-specific siRNA knockdown in WT VSMCs, thus excluding effects of any pre-existing differences in PCAF deficient cells. Our data correspond with a report that TNFα-induced NF-κB activity increases in human airway smooth muscle cells overexpressing PCAF (Clarke et al, 2008) and provide strong evidence for a wide effect of PCAF on inflammatory gene transcription.

The p65 subunit of NF-κB recruits co-activator PCAF and activates NF-κB-mediated gene transcription. In contrast, the NF-κB p50 subunit lacks the transcriptional activation domain and inhibits gene transcription (Driessler et al, 2004). Mice deficient of the NF-κB p50 subunit showed enhanced blood flow recovery after HLI as the result of increased monocyte recruitment to the perivascular space of collaterals (de Groot D. et al, 2010). Whereas arteriogenesis and monocyte recruitment is enhanced by NF-κB activation in NF-κB p50$^{-/-}$ mice, reduced regulation of the NF-κB p65 subunit in PCAF$^{-/-}$ mice could likely explain the impaired arteriogenesis by inhibition of monocyte recruitment. In WT mice, the monocyte population increased in the spleen and decreased in the bone marrow after HLI. This is in line with earlier reports that monocytes are mobilized from the bone marrow after HLI (Cochain et al, 2010). In that report, the pro-arteriogenic potential of monocytes was described to originate from a specific “pro-inflammatory” subtype, which is characterized by high expression of Ly6C. These Ly6Chi monocytes are recruited in the early stage of collateral remodeling (Capoccia et al, 2008; Cochain et al, 2010) and our data confirm that they are mobilized from the bone marrow in WT mice. In contrast, recruitment of monocytes proved to be severely impaired in PCAF$^{-/-}$ mice. PCAF$^{-/-}$ mice showed reduced numbers of circulating monocytes following HLI, particularly reduced numbers of Ly6Chi monocytes. Whereas monocytes migrated away from the bone marrow in WT mice, PCAF$^{-/-}$ mice showed an increase in bone marrow monocytes, suggesting a defect in monocyte mobilization. Concomitantly, 24 hours after HLI fewer monocytes were recruited to the collaterals in PCAF$^{-/-}$ mice. Monocytes stimulate arteriogenesis by secretion of growth factors and degradation of extracellular matrix at the site of collateral remodeling. Therefore, the lack of monocyte accumulation along collaterals likely contributes to the impaired arteriogenesis in PCAF$^{-/-}$ mice.

Besides monocytes, PCAF also affected numerous other leukocyte subtypes. In PCAF$^{-/-}$ mice, we demonstrated decreased numbers of circulating leukocytes involved in arteriogenesis, like T cells (Couffinhal et al, 1999) (predominantly activated

CD4+ T cells (Stabile et al, 2003; van Weel et al, 2007)), natural killer cells (van Weel et al, 2007) and regulatory T cells (Hellingman et al, 2012; Zouggari et al, 2009), and also in those cells that have not previously been implicated in arteriogenesis, including B cells. Furthermore, fewer dendritic cells were found in draining inguinal lymph nodes compared to WT mice, where the interaction between antigen-presenting dendritic cells and T cells takes place. Interestingly, nearly all subtypes were increased in the bone marrow of PCAF$^{-/-}$ mice, after HLI. This indicates that PCAF deficiency interferes with recruitment of pro-arteriogenic leukocytes from the bone marrow reservoir (Meisner & Price, 2010).

In conclusion, PCAF$^{-/-}$ mice demonstrated impaired collateral remodeling after HLI, together with a reduction in the number of native pre-existing collaterals present before arterial obstruction. PCAF deficiency resulted in altered expression of a large number of genes, including those in immune and inflammatory pathways, and an attenuated inflammatory response in multiple cell types involved in arteriogenesis. These findings indicate that PCAF is a key regulator in post-ischemic blood flow recovery by impacting the inflammatory processes required for robust arteriogenesis.

References

1. Bergmann CE, Hoefer IE, Meder B, Roth H, van Royen N., Breit SM, Jost MM, Aharinejad S, Hartmann S, and Buschmann IR (2006) Arteriogenesis depends on circulating monocytes and macrophage accumulation and is severely depressed in op/op mice. J Leukoc Biol 80: 59-65
2. Capoccia BJ, Gregory AD, and Link DC (2008) Recruitment of the inflammatory subset of monocytes to sites of ischemia induces angiogenesis in a monocyte chemoattractant protein-1-dependent fashion. J Leukoc Biol 84: 760-768
3. Chalothorn D and Faber JE (2010) Strain-dependent variation in collateral circulatory function in mouse hindlimb. Physiol Genomics 42: 469-479
4. Clarke DL, Sutcliffe A, Deacon K, Bradbury D, Corbett L, and Knox AJ (2008) PKCbetaII augments NF-kappaB-dependent transcription at the CCL11 promoter via p300/CBP-associated factor recruitment and histone H4 acetylation. J Immunol 181: 3503-3514
5. Cochain C, Rodero MP, Vilar J, Recalde A, Richart AL, Loinard C, Zouggari Y, Guerin C, Duriez M, Combadiere B, Poupel L, Levy BI, Mallat Z, Combadiere C, and Silvestre JS (2010) Regulation of monocyte subset systemic levels by distinct chemokine receptors controls post-ischaemic neovascularization. Cardiovasc Res 88: 186-195
6. Couffinhal T, Silver M, Kearney M, Sullivan A, Witzenbichler B, Magner M, Annex B, Peters K, and Isner JM (1999) Impaired collateral vessel development associated with reduced expression of vascular endothelial growth factor in ApoE-/- mice. Circulation 99: 3188-3198
7. Dai X and Faber JE (2010) Endothelial nitric oxide synthase deficiency causes collateral vessel rarefaction and impairs activation of a cell cycle gene network during arteriogenesis. Circ Res 106: 1870-1881
8. de Groot D., Haverslag RT, Pasterkamp G, de Kleijn DP, and Hoefer IE (2010) Targeted deletion of the inhibitory NF-kappaB p50 subunit in bone marrow-derived cells improves collateral growth after arterial occlusion. Cardiovasc Res 88: 179-185
9. Driessler F, Venstrom K, Sabat R, Asadullah K, and Schottelius AJ (2004) Molecular mechanisms of interleukin-10-mediated inhibition of NF-kappaB activity: a role for p50. Clin Exp Immunol 135: 64-73
10. Duclot F, Jacquet C, Gongora C, and Maurice T (2010) Alteration of working memory but not in anxiety or stress response in p300/CBP associated factor (PCAF) histone acetylase knockout mice bred on a C57BL/6 background. Neurosci Lett 475: 179-183
11. Grundmann S, Hoefer I, Ulusans S, van RN, Schirmer SH, Ozaki CK, Bode C, Piek JJ, and Buschmann I (2005) Anti-tumor necrosis factor-{alpha} therapies attenuate adaptive arteriogenesis in the rabbit. Am J Physiol Heart Circ Physiol 289: H1497-H1505
12. Guarani V, Deflorian G, Franco CA, Kruger M, Phng LK, Bentley K, Toussaint L, Dequiedt F, Mostoslavsky R, Schmidt MH, Zimmermann B, Brandes RP, Mione M, Westphal CH, Braun T, Zeiher AM, Gerhardt H, Dimmeler S, and Potente M (2011) Acetylation-dependent regulation of endothelial Notch signalling by the SIRT1 deacetylase. Nature 473: 234-238
13. Heil M and Schaper W (2004) Influence of mechanical, cellular, and molecular factors on collateral artery growth (arteriogenesis). Circ Res 95: 449-458
14. Heil M, Ziegelhoeffer T, Pipp F, Kostin S, Martin S, Clauss M, and Schaper W (2002) Blood monocyte concentration is critical for enhancement of collateral artery growth. Am J Physiol Heart Circ Physiol 283: H2411-H2419
15. Hellingman AA, Bastiaansen AJ, de Vries MR, Seghers L, Lijkwan MA, Lowik CW, Hamming JF, and Quax PH (2010) Variations in surgical procedures for hind limb ischaemia mouse models result in differences in collateral formation. Eur J Vasc Endovasc Surg 40: 796-803
16. Hellingman AA, van der Vlugt LE, Lijkwan MA, Bastiaansen AJ, Sparwasser T, Smits HH, Hamming JF, and Quax PH (2012) A limited role for regulatory T cells in post-ischemic neovascularization. J Cell Mol Med 16: 328-336
17. Hiasa K, Ishibashi M, Ohtani K, Inoue S, Zhao Q, Kitamoto S, Sata M, Ichiki T, Takeshita A, and Egashira K (2004) Gene transfer of stromal cell-derived factor-1alpha enhances ischemic vasculogenesis and angiogenesis via vascular endothelial growth factor/endothelial nitric oxide synthase-related pathway: next-generation chemokine therapy for therapeutic neovascularization. Circulation 109: 2454-2461
18. Ho TK, Tsui J, Xu S, Leoni P, Abraham DJ, and Baker DM (2010) Angiogenic effects of stromal cell-derived factor-1 (SDF-1/CXCL12) variants in vitro and the in vivo expressions of CXCL12 variants and CXCR4 in human critical leg ischemia. J Vasc Surg 51: 689-699

19. Hoefer IE, van Royen N, Rectenwald JE, Bray EJ, Abouhamze Z, Moldawer LL, Voskuil M, Piek JJ, Buschmann IR, and Ozaki CK (2002) Direct evidence for tumor necrosis factor-alpha signaling in arteriogenesis. Circulation 105: 1639-1641
20. Huang PH, Chen YH, Wang CH, Chen JS, Tsai HY, Lin FY, Lo WY, Wu TC, Sata M, Chen JW, and Lin SJ (2009) Matrix metalloproteinase-9 is essential for ischemia-induced neovascularization by modulating bone marrow-derived endothelial progenitor cells. Arterioscler Thromb Vasc Biol 29: 1179-1184
21. Imhof A, Yang XJ, Ogryzko VV, Nakatani Y, Wolffe AP, and Ge H (1997) Acetylation of general transcription factors by histone acetyltransferases. Curr Biol 7: 689-692
22. Itoh S, Ericsson J, Nishikawa J, Heldin CH, and ten Dijke P (2000) The transcriptional co-activator P/CAF potentiates TGF-beta/Smad signaling. Nucleic Acids Res 28: 4291-4298
23. Lee CW, Stabile E, Kinnaird T, Shou M, Devaney JM, Epstein SE, and Burnett MS (2004) Temporal patterns of gene expression after acute hindlimb ischemia in mice: insights into the genomic program for collateral vessel development. J Am Coll Cardiol 43: 474-482
24. Lenardo MJ and Baltimore D (1989) NF-kappa B: a pleiotropic mediator of inducible and tissue-specific gene control. Cell 58: 227-229
25. Lim JH, Lee YM, Chun YS, Chen J, Kim JE, and Park JW (2010) Sirtuin 1 modulates cellular responses to hypoxia by deacetylating hypoxia-inducible factor 1alpha. Mol Cell 38: 864-878
26. Liu L, Scolnick DM, Trievel RC, Zhang HB, Marmorstein R, Halazonetis TD, and Berger SL (1999) p53 sites acetylated in vitro by PCAF and p300 are acetylated in vivo in response to DNA damage. Mol Cell Biol 19: 1202-1209
27. Meier P, Gloekler S, Zbinden R, Beckh S, de Marchi SF, Zbinden S, Wustmann K, Billinger M, Vogel R, Cook S, Wenaweser P, Togni M, Windecker S, Meier B, and Seiler C (2007) Beneficial effect of recruitable collaterals: a 10-year follow-up study in patients with stable coronary artery disease undergoing quantitative collateral measurements. Circulation 116: 975-983
28. Meisner JK and Price RJ (2010) Spatial and temporal coordination of bone marrow-derived cell activity during arteriogenesis: regulation of the endogenous response and therapeutic implications. Microcirculation 17: 583-599
29. Menon BK, Bal S, Modi J, Sohn SI, Watson TW, Hill MD, Demchuk AM, and Goyal M (2012) Anterior temporal artery sign in CT angiography predicts reduced fatal brain edema and mortality in acute M1 middle cerebral artery occlusions. J Neuroimaging 22: 145-148
30. Miao F, Gonzalo IG, Lanting L, and Natarajan R (2004) In vivo chromatin remodeling events leading to inflammatory gene transcription under diabetic conditions. J Biol Chem 279: 18091-18097
31. Monraats PS, Rana JS, Zwinderman AH, de Maat MP, Kastelein JP, Agema WR, Doevendans PA, de Winter RJ, Tio RA, Waltenberger J, Frants RR, van der Laarse A, van der Wall EE, and Jukema JW (2005) -455G/A polymorphism and preprocedural plasma levels of fibrinogen show no association with the risk of clinical restenosis in patients with coronary stent placement. Thromb Haemost 93: 564-569
32. Pons D, Trompet S, de Craen AJ, Thijssen PE, Quax PH, de Vries MR, Wierda RJ, van den Elsen PJ, Monraats PS, Ewing MM, Heijmans BT, Slagboom PE, Zwinderman AH, Doevendans PA, Tio RA, de Winter RJ, de Maat MP, Iakoubova OA, Sattar N, Shepherd J, Westendorp RG, and Jukema JW (2011) Genetic variation in PCAF, a key mediator in epigenetics, is associated with reduced vascular morbidity and mortality: evidence for a new concept from three independent prospective studies. Heart 97: 143-150
33. Sartorelli V, Puri PL, Hamamori Y, Ogryzko V, Chung G, Nakatani Y, Wang JY, and Kedes L (1999) Acetylation of MyoD directed by PCAF is necessary for the execution of the muscle program. Mol Cell 4: 725-734
34. Schaper J, Konig R, Franz D, and Schaper W (1976) The endothelial surface of growing coronary collateral arteries. Intimal margination and diapedesis of monocytes. A combined SEM and TEM study. Virchows Arch A Pathol Anat Histol 370: 193-205
35. Schirmer SH, van Nooijen FC, Piek JJ, and van Royen N. (2009) Stimulation of collateral artery growth: travelling further down the road to clinical application. Heart 95: 191-197
36. Shao H, Tan Y, Eton D, Yang Z, Uberti MG, Li S, Schulick A, and Yu H (2008) Statin and stromal cell-derived factor-1 additively promote angiogenesis by enhancement of progenitor cells incorporation into new vessels. Stem Cells 26: 1376-1384
37. Sheppard KA, Rose DW, Haque ZK, Kurokawa R, McInerney E, Westin S, Thanos D, Rosenfeld MG, Glass CK, and Collins T (1999) Transcriptional activation by NF-kappaB requires multiple coactivators. Mol Cell Biol 19: 6367-6378

38. Shireman PK (2007) The chemokine system in arteriogenesis and hind limb ischemia. J Vasc Surg 45 Suppl A: A48-A56
39. Silke J and Brink R (2010) Regulation of TNFRSF and innate immune signalling complexes by TRAFs and cIAPs. Cell Death Differ 17: 35-45
40. Stabile E, Burnett MS, Watkins C, Kinnaird T, Bachis A, la Sala A, Miller JM, Shou M, Epstein SE, and Fuchs S (2003) Impaired arteriogenic response to acute hindlimb ischemia in CD4-knockout mice. Circulation 108: 205-210
41. Stabile E, Kinnaird T, la Sala A, Hanson SK, Watkins C, Campia U, Shou M, Zbinden S, Fuchs S, Kornfeld H, Epstein SE, and Burnett MS (2006) CD8+ T lymphocytes regulate the arteriogenic response to ischemia by infiltrating the site of collateral vessel development and recruiting CD4+ mononuclear cells through the expression of interleukin-16. Circulation 113: 118-124
42. Tusher VG, Tibshirani R, and Chu G (2001) Significance analysis of microarrays applied to the ionizing radiation response. Proc Natl Acad Sci U S A 98: 5116-5121
43. van Oostrom MC, van Oostrom O, Quax PH, Verhaar MC, and Hoefer IE (2008) Insights into mechanisms behind arteriogenesis: what does the future hold? J Leukoc Biol 84: 1379-1391
44. van Weel V, Toes RE, Seghers L, Deckers MM, de Vries MR, Eilers PH, Sipkens J, Schepers A, Eefting D, van H, V, van Bockel JH, and Quax PH (2007) Natural killer cells and CD4+ T-cells modulate collateral artery development. Arterioscler Thromb Vasc Biol 27: 2310-2318
45. Voskuil M, Hoefer IE, van Royen N, Hua J, de GS, Bode C, Buschmann IR, and Piek JJ (2004) Abnormal monocyte recruitment and collateral artery formation in monocyte chemoattractant protein-1 deficient mice. Vasc Med 9: 287-292
46. Wang S, Zhang H, Dai X, Sealock R, and Faber JE (2010) Genetic architecture underlying variation in extent and remodeling of the collateral circulation. Circ Res 107: 558-568
47. Yamauchi T, Yamauchi J, Kuwata T, Tamura T, Yamashita T, Bae N, Westphal H, Ozato K, and Nakatani Y (2000) Distinct but overlapping roles of histone acetylase PCAF and of the closely related PCAF-B/GCN5 in mouse embryogenesis. Proc Natl Acad Sci U S A 97: 11303-11306
48. Yang M and Odgren PR (2005) Molecular cloning and characterization of rat CCL9 (MIP-1gamma), the ortholog of mouse CCL9. Cytokine 31: 94-102
49. Zhang H, Prabhakar P, Sealock R, and Faber JE (2010) Wide genetic variation in the native pial collateral circulation is a major determinant of variation in severity of stroke. J Cereb Blood Flow Metab 30: 923-934
50. Zouggari Y, Ait-Oufella H, Waeckel L, Vilar J, Loinard C, Cochain C, Recalde A, Duriez M, Levy BI, Lutgens E, Mallat Z, and Silvestre JS (2009) Regulatory T cells modulate postischemic neovascularization. Circulation 120: 1415-1425

Supplementary figures

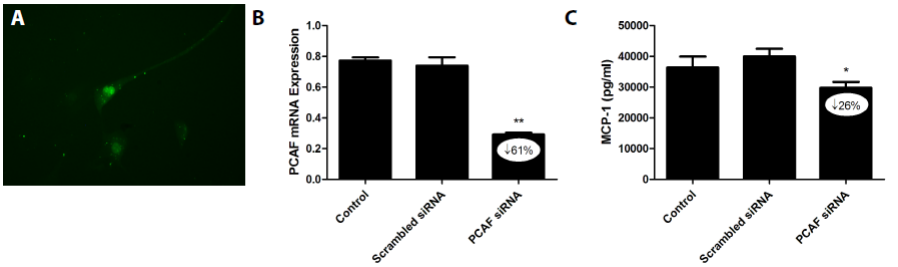

Figure 1. PCAF knockdown by siRNA in vascular smooth muscle cells. A. Vascular smooth muscle cells (VMSCs) were transfected with nontarget fluorescent siGlow (Dharmacon) to test transfection efficiency, using Lipofectamine 2000 according to the manufacturer's instructions. VSMCs were visualized on a Leica fluorescence microscope. B. VSMCs were plated and transfected with control short-interfering RNA (siRNA) or a combination of 4 siRNAs directed towards PCAF for 4 hours. Untransfected VMSCs were used as control.
VSMCs were incubated with LPS (1 ng/ml) for 24 hours. To confirm PCAF knockdown, PCAF mRNA was measured by real-time quantitative PCR. Levels were normalized against the expression of HPRT1. PCAF specific siRNA reduced PCAF expression with 61% in comparison to scrambled siRNA. C. Cell-free supernatant of LPS stimulated VSMCs was collected for MCP-1 quantification, measured by ELISA. Transfection with PCAF specific siRNA inhibited MCP-1 production of VSMCs in comparison to scrambled siRNA. All samples were performed in triplicates. *P < .05, **P < .01, scrambled siRNA versus PCAF siRNA.

Figure 2. Differential inflammatory gene expression in PCAF$^{-/-}$ and WT mice. Heatmap of differentially expressed inflammatory genes in adductor muscle group of PCAF$^{-/-}$ and WT mice, 1 day after HLI. Gene definitions containing any of these criteria (interleukin, chemokine, interferon, TGF, TNF, NFKB) were selected. Included are genes that were significantly different between PCAF$^{-/-}$ and WT mice (q-value < 5). Data are presented as the fold change in expression between day 1 and average preoperative baseline levels, generating t1/t0avg ratios. Red indicates increased and green indicates reduced expression relative to average baseline levels.

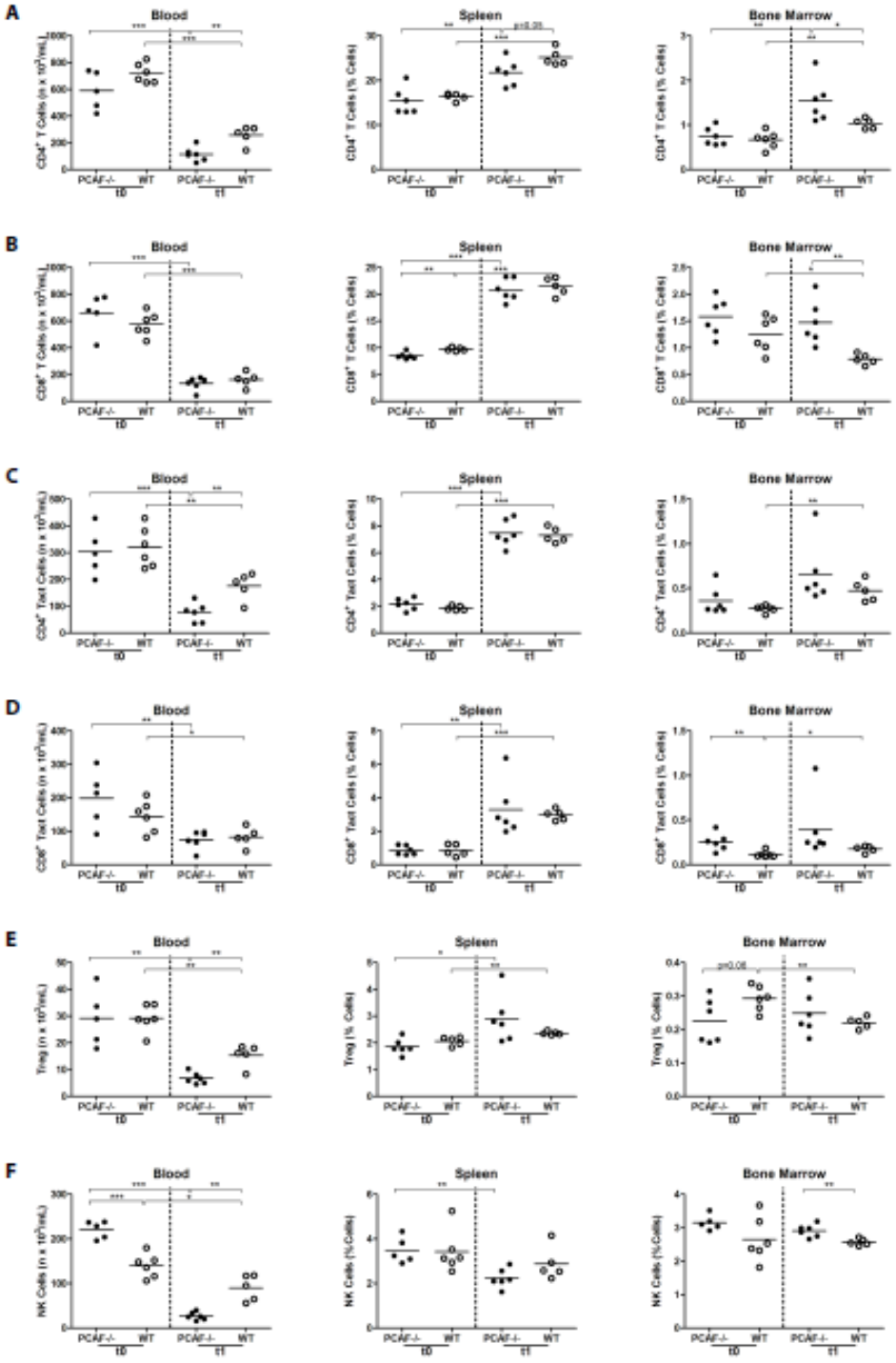
A
Blood
Spleen
Bone Marrow
CD4+ T Cells (n x 10³/mL)
CD4+ T Cells (% Cells)
B
Blood
Spleen
Bone Marrow
CD8+ T Cells (n x 10³/mL)
CD8+ T Cells (% Cells)
C
Blood
Spleen
Bone Marrow
CD4+ Tact Cells (n x 10³/mL)
CD4+ Tact Cells (% Cells)
D
Blood
Spleen
Bone Marrow
CD8+ Tact Cells (n x 10³/mL)
CD8+ Tact Cells (% Cells)
E
Blood
Spleen
Bone Marrow
Treg (n x 10³/mL)
Treg (% Cells)
F
Blood
Spleen
Bone Marrow
NK Cells (n x 10³/mL)
NK Cells (% Cells)
PCAF-/-
WT
t0
t1

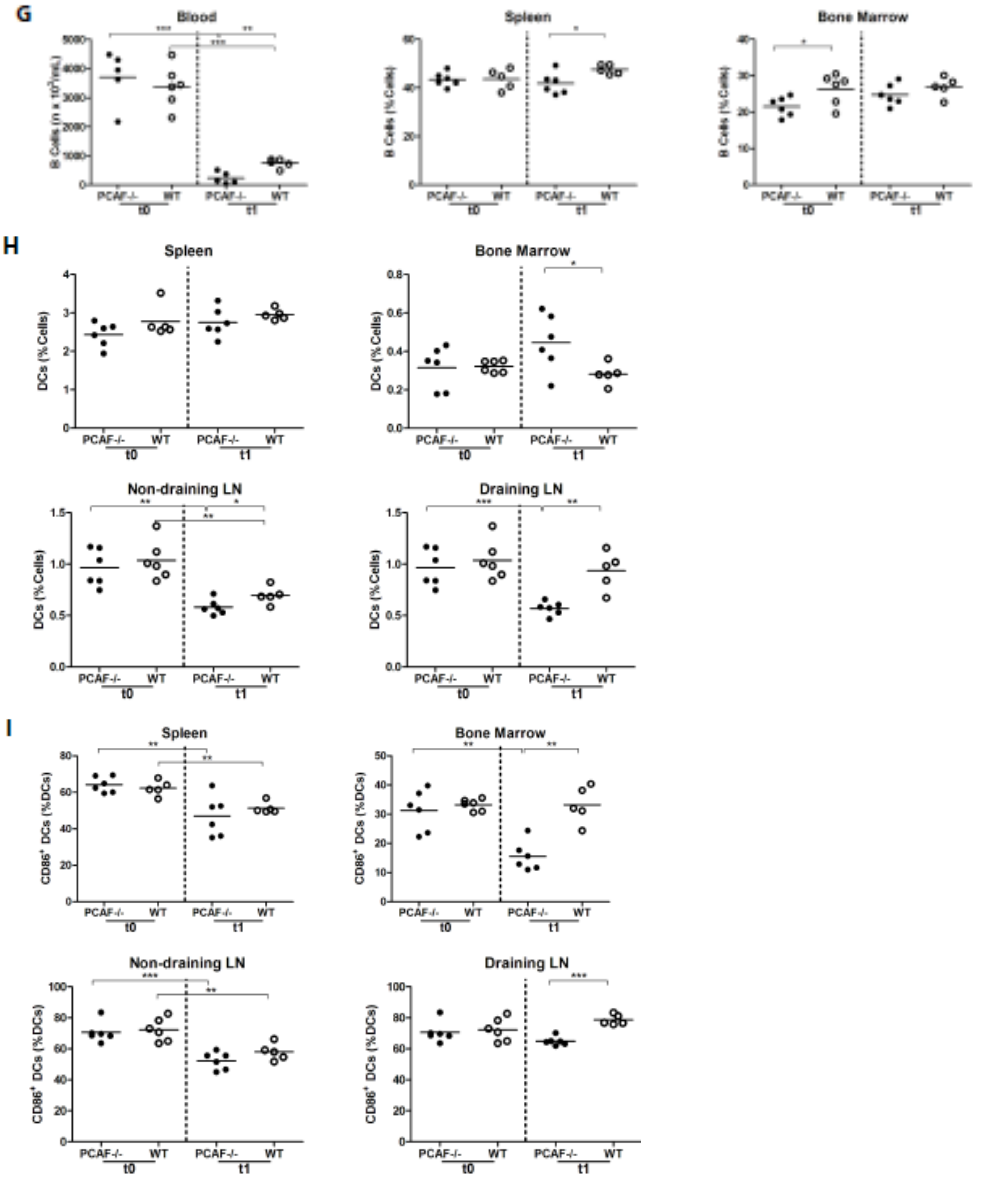

Figure 3. Leukocyte subtypes in PCAF$^{-/-}$ and WT mice after HLI. Flow cytometry analysis of lymphocytes in blood (nx10^3/mL), spleen and bone marrow (% of total cells). In succession, values are presented for (A) CD4+ T helper cells, (B) CD8+ cytotoxic T cells, (C) activated CD4+ T helper cells, (D) activated CD8+ cytotoxic T cells, (E) regulatory T cells (Treg), (F) Natural Killer (NK) cells and (G) B lymphocytes. (H) Dendritic cells (DCs) in spleen, bone marrow, nondraining and draining (inguinal) lymph nodes (LN). (I) Activated DCs in spleen, bone marrow, non-draining and draining (inguinal) lymph nodes.

Symbol	Gene Name	PCAF-/-	WT		Ratio PCAF$^{+/-}$ vs WT
		logFC	logFC	q-value	FC
Arg1	arginase 1, liver	1,55	3,11	4,39	0,34
Pdk4	pyruvate dehydrogenase kinase, isoenzyme 4	0,17	1,29	3,00	0,46
Ptpn6	protein tyrosine phosphatase, non-receptor type 6, transcript variant 2	0,55	1,54	0,86	0,50
Lst1		0,37	1,36	0,86	0,50
Anxa2	annexin A2 (Anxa2), mRNA.	0,39	1,37	0,69	0,51
Serpinb1a	serine (or cysteine) peptidase inhibitor, clade B, member 1a	0,31	1,28	1,23	0,51
Slfn1	schlafen 1	0,79	1,74	1,66	0,52
Mmp9	matrix metallopeptidase 9	0,07	1,01	0,69	0,52
Cotl1	coactosin-like 1	0,66	1,60	1,23	0,52
Cd52	CD52 antigen	1,41	2,33	4,39	0,53
Tagln2	transgelin 2	0,23	1,15	0,86	0,53
Ccl9	chemokine (C-C motif) ligand 9	1,91	2,81	3,60	0,54
LOC100046120	PREDICTED: similar to clusterin	1,06	1,94	1,23	0,54
Angptl4	angiopoietin-like 4	0,43	1,31	3,60	0,54
Cfp	complement factor properdin	0,37	1,23	0,40	0,55
Cotl1	coactosin-like 1	0,42	1,25	0,59	0,56
Kcnab2	potassium voltage-gated channel, shaker-related subfamily, beta member 2	0,37	1,16	0,59	0,58
LOC100044439	PREDICTED: similar to cytochrome P450 CYP4F18	0,40	1,19	1,66	0,58
Sirpa	signal-regulatory protein alpha	0,55	1,33	1,94	0,58
Fbxo32	F-box protein 32	0,86	1,63	4,39	0,59
Alox5ap	arachidonate 5-lipoxygenase activating protein	1,13	1,87	1,94	0,60
Arhgdib	Rho, GDP dissociation inhibitor (GDI) beta	0,32	1,04	1,23	0,61
Emilin2	elastin microfibril interfacer 2	0,10	0,82	0,86	0,61
Lrrc33	leucine rich repeat containing 33	0,42	1,12	0,86	0,62
Fbxl22	F-box and leucine-rich repeat protein 22	0,26	0,96	2,42	0,62
Emilin2	elastin microfibril interfacer 2	0,12	0,80	1,94	0,62
Cyth4	cytohesin 4	0,74	1,41	4,39	0,63
Laptm5	lysosomal-associated protein transmembrane 5	0,92	1,59	0,98	0,63
Sdc3	syndecan 3	0,07	0,73	0,86	0,64
Ly6e	lymphocyte antigen 6 complex, locus E	0,01	0,66	0,33	0,64
Hdac4	histone deacetylase 4	0,02	0,66	0,00	0,64
Dok2	docking protein 2	0,50	1,14	1,94	0,64
Fcgr4	Fc receptor, IgG, low affinity IV	1,63	2,26	3,60	0,64
Alox5ap	arachidonate 5-lipoxygenase activating protein	0,85	1,48	2,42	0,65
Cap1	CAP, adenylate cyclase-associated protein 1	0,26	0,89	0,98	0,65
Tgfbi	transforming growth factor, beta induced	0,36	0,99	3,00	0,65
Aif1	allograft inflammatory factor 1	0,23	0,84	1,23	0,65
Mcm5	minichromosome maintenance deficient 5, cell division cycle 46	0,07	0,68	0,00	0,65
Fes	feline sarcoma oncogene	0,33	0,95	0,45	0,65
Gnb2	guanine nucleotide binding protein (G protein), beta 2	0,07	0,68	0,00	0,66
Cyba	cytochrome b-245, alpha polypeptide	0,56	1,17	1,23	0,66
Grn	granulin	0,21	0,81	0,00	0,66
Fxyd5	FXYD domain-containing ion transport regulator 5	0,78	1,38	3,60	0,66
Cdh15	cadherin 15	0,09	0,69	0,33	0,66
Rabgef1	RAB guanine nucleotide exchange factor	0,24	0,82	0,45	0,67
Oas1g	2'-5' oligoadenylate synthetase 1G	0,04	0,62	0,98	0,67
Arrb2	arrestin, beta 2	0,04	0,62	0,40	0,67
Emp3	epithelial membrane protein 3	0,33	0,90	3,60	0,67
Sh3bgrl3	SH3 domain binding glutamic acid-rich protein-like 3	0,60	1,16	1,23	0,68
S100a11	S100 calcium binding protein A11	0,54	1,11	4,39	0,68

Table 1. List of differentially expressed genes in the adductor muscle group of PCAF$^{-/-}$ and WT mice. Data are presented as the log fold change in expression between day 1 after HLI and average preoperative baseline levels, generating t1/t0avg ratios. Listed are the top 50 genes which showed an impaired upregulation in PCAF$^{-/-}$ mice compared to WT mice. Q-values less than 5% were considered significant. FC = fold change.

Symbol	Gene Name	PCAF-/-	WT	
		logFC	logFC	q-value
Ccl9	chemokine (C-C motif) ligand 9	1,91	2,81	3,60
Tgfbi	transforming growth factor, beta induced	0,36	0,99	3,00
Tnfrsf19	tumor necrosis factor receptor superfamily, member 19	-0,64	-0,04	1,66
C1qtnf9	C1q and tumor necrosis factor related protein 9	-0,95	-0,50	3,00
LOC100041504	PREDICTED: similar to beta chemokine Exodus-2	-0,16	0,27	3,60
Cxcl12	chemokine (C-X-C motif) ligand 12, transcript variant 3	-0,58	-0,16	3,60
C1qtnf2	C1q and tumor necrosis factor related protein 2	-0,57	-0,16	0,00
Traf2	Tnf receptor-associated factor 2	-0,28	0,12	3,60
Ifitm3	interferon induced transmembrane protein 3	1,00	1,39	2,42
Tgfb3	transforming growth factor, beta 3	-0,40	-0,02	4,39
Il8ra	interleukin 8 receptor, alpha	0,07	0,43	0,98
Ifngr2	interferon gamma receptor 2	-0,48	-0,15	1,94
Il3ra	interleukin 3 receptor, alpha chain	-0,02	0,30	0,69
C1qtnf5	C1q and tumor necrosis factor related protein 5, transcript variant 1	-0,11	0,19	0,33
Traf3	Tnf receptor-associated factor 3, transcript variant 1	-0,26	0,04	4,39
Tnfaip8l2	tumor necrosis factor, alpha-induced protein 8-like 2	0,07	0,36	1,94
Ifit3	interferon-induced protein with tetratricopeptide repeats 3	-0,23	0,06	4,39
Irf7	interferon regulatory factor 7	0,00	0,24	1,94
Fadd	Fas (TNFRSF6)-associated via death domain	-0,04	0,19	4,39
Tnfrsf11a	tumor necrosis factor receptor superfamily, member 11a	0,14	0,37	2,42
Prkra	protein kinase, interferon inducible double stranded RNA dependent activator	-0,14	0,08	4,39
Il17rc	interleukin 17 receptor C	0,01	0,23	0,98
Trap1	TNF receptor-associated protein 1	-0,10	0,11	1,66
Tnf	tumor necrosis factor	-0,08	0,11	1,94
Il18	interleukin 18	-0,12	0,04	4,39

Symbol	Gene Name	PCAF-/-	WT	
		logFC	logFC	q-value
Irak1	interleukin-1 receptor-associated kinase 1	0,18	0,00	1,66
Ilf3	interleukin enhancer binding factor 3, transcript variant 3	0,19	0,00	0,98
Tgfbr2	transforming growth factor, beta receptor II, transcript variant 1	0,47	0,24	3,60
LOC100048583	PREDICTED: similar to interferon-inducible protein 203, transcript variant 1	0,16	-0,08	0,33
Ccrl1	chemokine (C-C motif) receptor-like 1	-0,15	-0,42	3,00
LOC545396	PREDICTED: similar to TGF beta-inducible nuclear protein 1	-0,06	-0,33	3,00
Nfkbia	nuclear factor of kappa light polypeptide gene enhancer in B-cells inhibitor, alpha	0,36	0,06	3,60
Irf2bp2	PREDICTED: interferon regulatory factor 2 binding protein 2	0,09	-0,22	3,00
Nkiras1	NFKB inhibitor interacting Ras-like protein 1	0,15	-0,17	0,00
Ccl19	chemokine (C-C motif) ligand 19	1,02	0,68	0,40
Il15ra	interleukin 15 receptor, alpha chain, transcript variant 2	0,20	-0,15	2,42
Il6ra	interleukin 6 receptor, alpha	0,69	0,21	1,66
Il4i1	interleukin 4 induced 1	-0,39	-1,10	0,00
LOC100044430	PREDICTED: similar to Interferon activated gene 205	1,27	0,50	1,23
Cxcl1	chemokine (C-X-C motif) ligand 1	2,93	1,45	1,66

Table 2. List of significantly differentially expressed inflammatory genes in the adductor muscle group of PCAF$^{-/-}$ and WT mice. Data are presented as the log fold change in expression between day 1 after HLI and average preoperative baseline levels, generating t1/t0avg ratios. Gene definitions containing any of these criteria (interleukin, chemokine, interferon, TGF, TNF, NFKB) were selected. Q-values less than 5% were considered significant. FC = fold change.